Trapping of Charged Gold Adatoms by Dimethyl Sulfoxide on a Gold Surface

Zhijing Feng,[†,§] Simone Velari,[‡] Albano Cossaro,[§] Carla Castellarin-Cudia,[§] Alberto Verdini,[§] Erik Vesselli,[†,§] Carlo Dri,[*,†,§] Maria Peressi,[†,⊥,∥] Alessandro De Vita,[#,‡] and Giovanni Comelli[†,§]

[†]Physics Department, University of Trieste, Via A. Valerio 2, 34127 Trieste, Italy, [‡]Engineering and Architecture Department, University of Trieste, Via A. Valerio 6/1, 34147 Trieste, Italy, [§]TASC Laboratory, Istituto Officina dei Materiali CNR-IOM, S.S. 14 km 163.5, 34149 Trieste, Italy, [∥]CNR-IOM DEMOCRITOS, Area Science Park, S.S. 14 km 163.5, 34149 Trieste, Italy, [⊥]Consorzio Interuniversitario Nazionale per la Scienza e la Tecnologia dei Materiali (INSTM), Unità di ricerca di Trieste, Piazzale Europa 1, 34128 Trieste, Italy, and [#]Department of Physics, King's College London, Strand, London WC2R 2LS, United Kingdom

ABSTRACT We report the formation of dimethyl sulfoxide (DMSO) molecular complexes on Au(111) enabled by native gold adatoms unusually linking the molecules *via* a bonding of ionic nature, yielding a mutual stabilization between molecules and adatom(s). DMSO is a widely used polar, aprotic solvent whose interaction with metal surfaces is not fully understood. By combining X-ray photoelectron spectroscopy, low temperature scanning tunneling microscopy, and density functional theory (DFT) calculations, we show that DMSO molecules form complexes made by up to four molecules arranged with adjacent oxygen terminations. DFT calculations reveal that most of the observed structures are accurately reproduced if, and only if, the negatively charged oxygen terminations are linked by one or two positively charged Au adatoms. A similar behavior was previously observed only in nonstoichiometric organic salt layers, fabricated using linkage alkali atoms and strongly electronegative molecules. These findings suggest a motif for anchoring organic adlayers of polar molecules on metal substrates and also provide nanoscale insight into the interaction of DMSO with gold.

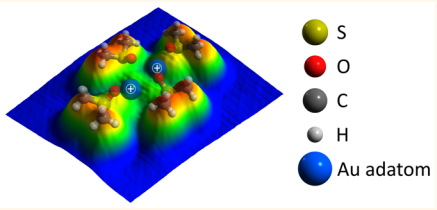

KEYWORDS: dimethyl sulfoxide · DMSO · scanning tunneling microscopy · photoemission spectroscopy · density functional theory · gold · adatom

The ability to control the structural and electronic properties of (hetero)-organic assemblies on metal surfaces is the key issue for the design of efficient devices in organic electronics, which has triggered a significant effort in the recent years in this field.[1−4] Gold single crystal terminations are often adopted for their inertness to support the growth of 2D supramolecular architectures. In particular, on the Au(111) substrate, when suitable tectons[5] are used, the molecule−substrate coupling is relatively weak, and manifold synthons[6] involving noncovalent[7−10] or metal−organic[11−15] interactions have been exploited to program the desired properties of the final architectures. Moreover, the (111) face of gold is the most stable one, and molecular interactions on and with this substrate are of great importance since, in most applications, where polycrystalline gold electrodes or clusters are involved, (111)-terminated facets predominate.[16,17]

Despite being inert ("noble") in its bulk form, gold exhibits rich catalytic properties and ligand chemistry when in the form of small clusters composed by tens of atoms down to single atoms, where gold is under-coordinated with respect to its bulk form.[18,19] The interest in nanogold chemistry has seen a significant upswing only in the last decades, and nowadays reaches well beyond fundamental research, finding valuable applications ranging from real catalysts for oxidation reactions up to radiosensitization agents in cancer therapy.[20,21] In particular, heterogeneous catalysts based on highly dispersed gold have been widely investigated, and a remarkable understanding of the structure−activity relationship at the nanoscale, as well as of the role of the catalyst support, has been achieved in the last 20 years.[18,22−24]

At the intersection between these two seemingly opposite worlds, *i.e.*, the inertness of gold substrates and the nanoscale reactivity of gold clusters, an exciting route opens up to novel binding motifs that can encode specific properties of the supramolecular assemblies, based on gold adatoms as molecular linkers. In fact, on the Au(111) surface, low-coordinated atoms are natively

* Address correspondence to dri@iom.cnr.it.

Received for review April 16, 2015 and accepted June 16, 2015.

Published online June 16, 2015
10.1021/acsnano.5b02284

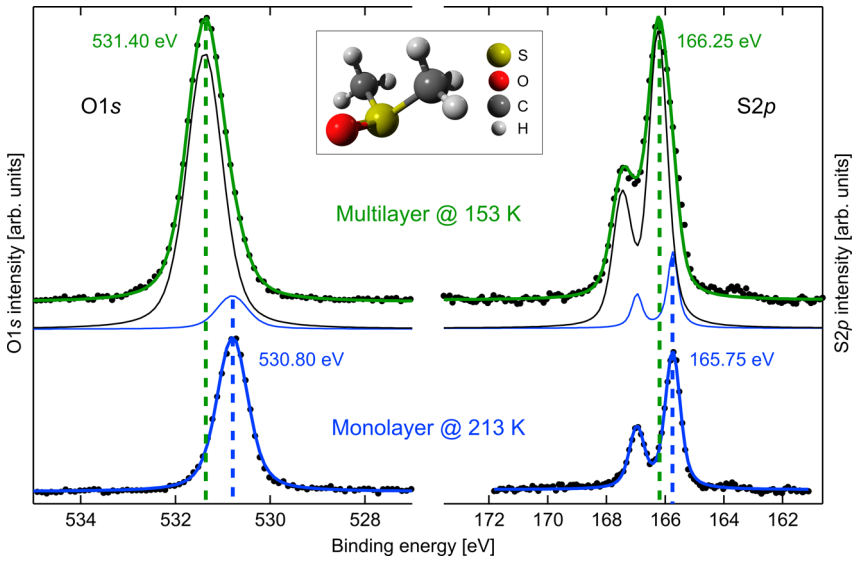

Figure 1. O 1s and S 2p spectra ($h\nu$ = 650 eV) acquired on the multilayer (153 K, top spectra, green) and on the monolayer (213 K, bottom spectra, blue) phase. The uncertainty on the absolute binding energy values is ±0.05 eV. Individual components, obtained from the fit, are superimposed on the spectra. The inset shows a ball and stick model of the DMSO molecule (yellow, sulfur; red, oxygen; gray, carbon; white, hydrogen).

available, since the higher density of gold atoms in the first atomic layer induces a periodic displacement of the atoms out of the surface plane along the soliton walls of the herringbone reconstruction.[25,26] On this surface, extraction and stabilization of native gold adatoms can be induced by interaction of organic molecules with the Au(111) surface, as observed for instance with molecules containing cyano (CN) groups,[14,15,27] organophosphorus compounds,[28,29] porphyrin or phthalocyanine derivatives,[30−32] and molecules containing very electronegative substituents such as chlorine[33] or sulfur.[34,35] Apart from thiols (R−SH), which are known to induce deep restructuring of the gold surface by covalently binding to this substrate,[36−40] to our knowledge there are only few examples where 2D or 1D supramolecular architectures are stabilized by native gold adatoms as linkers. In these cases, the Au adatoms appear to play the well-known role of transition metal linkers, where reported substituents are often distinctively electronegative.[1,41,42] An alternative linkage method that has been recently explored involves alkali metal linkers.[43] Together with providing tunable interfacial electronic properties,[44] they also allow more flexible bonding geometries due to the ionic character of the metal−molecule interaction, in contrast to the directional coordination enforced by the shape of the transition metal d orbitals.[1,13] Gold can be seen as a half-filled s shell element, in analogy to alkali metals: this suggests the idea that undercoordinated gold adatoms could also display ionic behavior, particularly when interacting with polarized but neutral molecules, although this has not been reported to date. However, the observation of such ionic gold linkers by scanning tunneling microscopy (STM) experiments could be hindered by the small ionic radius of oxidized Au, and by the Au linker adatoms being possibly located below the plane of the molecular adsorbates and thereby hidden.

In this work, we substantiate this physical picture by depositing on a gold surface a very simple polar molecule, dimethyl sulfoxide ($(CH3)_2SO$, DMSO, see inset in Figure 1), which is constituted by a sulfinyl (S═O) group and two methyl (CH_3) groups bound to the sulfur atom, and it is characterized by a large dipole moment (3.96 D).[45] DMSO is an aprotic solvent, produced as a byproduct of the paper industry and widely employed both in laboratory and in industrial processes. It finds numerous applications in the electronics industry,[46,47] in biology and medicine as a radio- and cryo-protective agent for cells and tissues,[48] as well as a percutaneous drug penetration enhancer.[49]

By means of X-ray photoelectron and near-edge absorption spectroscopy (XPS and NEXAFS), and by extensive Low Temperature Scanning Tunneling Microscopy measurements (LT-STM) of DMSO on Au(111) from multilayer to submonolayer molecular coverages, we show how the adsorption of this molecule is characterized by the formation of characteristic molecular complexes composed of three or four DMSO molecules. The latter appear in the STM images to be linked through their negatively charged, and thus presumably mutually repelling, terminations. This puzzling supramolecular structure has been rationalized by comparing the experimental STM images with simulated ones, obtained by density functional theory calculations (DFT). As it will be shown, our results clearly indicate that the majority of the observed complexes can be accurately reproduced if, and only if, the negatively charged oxygen terminations are linked by one or two Au adatoms, which are "invisible" in the STM images.

RESULTS AND DISCUSSION

To our knowledge, only very few experimental works have characterized the adsorption of DMSO on metal surfaces, in ultrahigh vacuum (UHV)[50−53] or in solution[51,54,55] environments. In particular, on Au(100) and Au(111), the structural properties of the DMSO−gold interface have been probed by STM, but only tentative models were put forward on the basis of poorly resolved features in the STM images.[51,56]

To characterize the adsorption of DMSO, we have first monitored the O 1s and S 2p photoemission spectral features of films obtained by depositing the molecules at different temperatures T_s of the Au(111) sample in the 153 K < T_s < 300 K range. Curve fitting reveals the presence of multilayer components for T_s < 193 K (top spectra in Figure 1), whereas a decreasing coverage starting from the full monolayer is observed in the 193 K < T_s < 300 K range. It is to be noted that, in the latter temperature range, both S 2p and O 1s spectra are always characterized by a single component (bottom spectra of Figure 1), and no significant changes in the profile shapes are observed with decreasing coverage. In the S 2p spectra, minor features are visible below 165 eV, related to X-ray induced damage, as discussed in the Supporting Information. In Figure 1, the deconvolution profiles obtained by the fitting procedure highlight a binding energy shift between the monolayer (blue) and multilayer (black) components, arising from the screening effect of the metallic substrate.

The shift has comparable values, within 0.1 eV, for both the S 2p and O 1s features. Both the S and O atoms of the DMSO molecule have an electron lone pair and can therefore act as electron-donors in binding to the substrate or to an adjacent molecule. In the latter case, as compared to a noninteracting molecule, an increase in the binding energy of the donating atom is expected. On these bases, in an early paper, Su and Faller[57] measured the difference between the O 1s and S 2p binding energies, ΔE_b, for several metal−DMSO complexes, attempting to determine from this quantity whether the metal−molecule bonding occurred through the oxygen atom, the sulfur atom, or both. This method was adopted to rationalize the XPS data for the adsorption of DMSO on Au(100) and Pt(111),[52,55] where bi- and monodentate configurations have been found, respectively. By adopting this approach, the change in ΔE_b we found (≈ 0.1 eV, not significant within our errors) suggests that, as it occurs on the Au(100) surface, also in the Au(111) case DMSO adsorbs interacting with both its donor terminations to the metal. However, an important aspect, which was not discussed in the cited works, has also to be considered. Indeed, the supramolecular assembly at both monolayer and multilayer stages can be driven by the formation of intermolecular hydrogen bonds,

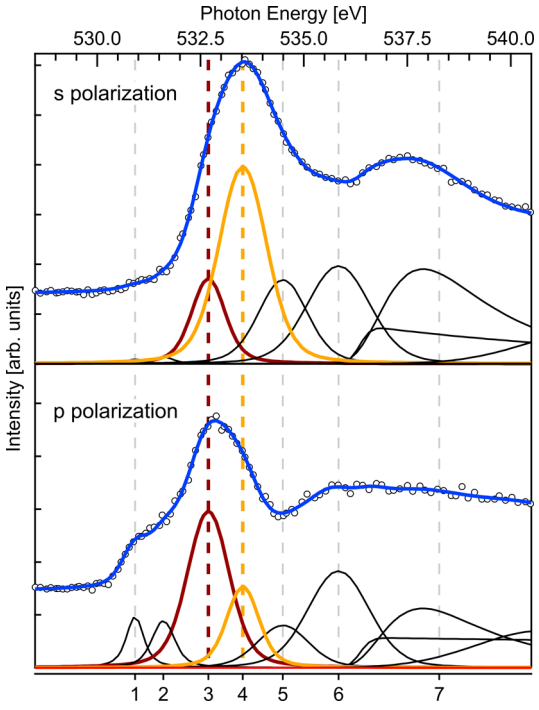

Figure 2. Linear dichroism NEXAFS spectra at the O 1s edge for two different synchrotron light polarizations (s polarization, parallel to the surface; p polarization, perpendicular to the surface) of DMSO/Au(111) after annealing at 213 K. The main peaks, 3 and 4, are located at 532.7 and 533.5 eV, respectively. Peaks 1 and 2 are assigned to impurities or beam induced damage, whereas peaks 5−7 are related to oxygen Rydberg states[59] (see Supporting Information for a discussion of the assignments).

which affects the binding energy of the termination involved in the interaction. If we assume that the structure of the DMSO multilayer resembles the crystalline phase, where oxygen−methyl interactions are present,[58] a shift toward higher binding energies is expected in addition to the screening effect of the substrate. The proper reference value of ΔE_b for a noninteracting DMSO molecule should therefore be provided from spectra acquired in the gas phase, which are not available. Moreover, the O−CH_3 affinity could also drive the assembly of the monolayer phase. These observations indicate that it is not possible to unambiguously infer a bidentate DMSO−metal bonding from the observed small ΔE_b, and therefore call for further investigations to characterize the nature of the molecule−metal and molecule−molecule interactions.

To tackle this question, we also investigated the DMSO adsorption geometry at the monolayer stage by means of NEXAFS measurements. Figure 2 reports the O 1s light polarization-dependent NEXAFS spectra, measured on a DMSO monolayer grown at 213 K. The fit of the curves reveals the presence of distinct components, showing a clear dichroic effect, thus suggesting that the molecules adsorb on the surface with preferential orientation. A detailed discussion with a tentative assignment of all the main peaks of the

spectra is provided in the Supporting Information, on the basis of the few works present in the literature regarding the electronic structure of DMSO empty states. It is to be noted that similar conclusions can be drawn from NEXAFS spectra acquired at higher temperatures (also shown in the Supporting Information).

Our spectra resemble the ones taken in both the gas[59] and liquid phase,[60] apart from a finer structure observable in our case, possibly due to the fact that in both nonsolid phases the molecules are randomly oriented and dichroic effects are not measurable.

In a nutshell, comparison with gas phase spectra[60,61] identifies peak 3 (532.7 eV) as due to a transition from the O 1s to the LUMO, which has a π^* character, and is expected to have maximum intensity when the photon polarization is perpendicular to the S═O bond. Conversely, peak 4 (533.5 eV) shows opposite polar dependence and can be assigned to the σ^* transition of the same bond. By comparing the intensities of this peak at the two polarization angles, we determined that the S═O bond is tilted by 25 ± 10° with respect to the surface plane.[62]

Summarizing the information obtained from XPS and NEXAFS, on one side, XPS indicates that DMSO could possibly interact with the metal both *via* the S and O atoms, whereas the role of hydrogen bonding remains to be assessed. On the other, at the same time, NEXAFS reveals that the S═O bond appears to be significantly raised from the surface plane. These two apparently conflicting findings call for a deeper investigation of the adsorption of DMSO, and in order to shed light on this point, we performed high-resolution LT-STM imaging of molecular layers.

Due to the weak bonding of the molecules in the multilayer, STM imaging could not be carried out on this phase. Conversely, the structure of the monolayer phase, obtained by annealing the multilayer at 193 K, could be readily imaged and is discussed in the Supporting Information. Here, we focus on the submonolayer phases. Interestingly, after annealing the monolayer phase to 233 K, thereby desorbing a large part of the DMSO molecules, the surface appears as shown in the STM image in Figure 3a. From the high-resolution insets (Figure 3b,c), the features corresponding to the molecular structure of DMSO can be straightforwardly identified: the two brighter protrusions correspond to the methyl groups, whereas the less intense one can be assigned to the oxygen atom. The appearance also suggests that the molecule is sitting in an "inverted umbrella" geometry, *i.e.*, with the S atom directly interacting with the Au surface. From these considerations, the dominant structural motif of this layer appears to be a complex of four DMSO molecules (hereafter referred to as *square*), together with a smaller number of isolated, single DMSO molecules.

Within the *square* complex, it appears that DMSO favors a geometry where the oxygen atoms are located

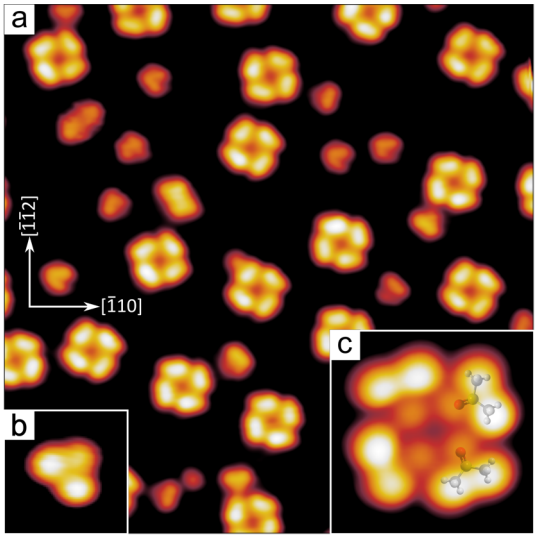

Figure 3. (a) STM image (12.82 × 12.82 nm^2) showing the *square* complexes formed by annealing the DMSO/Au(111) multilayer phase to 233 K. Panels b (1.00 × 1.00 nm^2) and c (1.60 × 1.60 nm^2) are high-resolution details of a single isolated DMSO molecule and a *square* complex, respectively. Transparent ball and stick models are superimposed to guide the eye in the identification of the single molecules. Image parameters: (a) V_s = 100 mV, I_t = 100 pA; (b) V_s = 50 mV, I_t = 100 pA; (c) V_s = 100 mV, I_t = 50 pA.

close to each other, a configuration that should intuitively be relatively unstable, due to mutual repulsion of the oxygen atoms, even though a weak attractive interaction between the methyl groups and the oxygen atoms of adjacent molecules could instead favor the stability of the complex. To investigate the stability of the *squares*, we performed extensive manipulation experiments, both by scanning at high bias voltages (*i.e.*, within 3 V) and by applying voltage pulses on top of the complexes.

What we found is that the *square* can be easily rotated as a whole on the surface plane, but it is impossible to separate its constituent molecules without irreversible damage, *i.e.*, the fragments observed on the surface after strong manipulation attempts have completely lost the characteristic appearance, in terms of size and shape, of the DMSO molecules. Therefore, the interaction between the DMSO molecules within the *squares* appears to be remarkably strong and dominated by the attractive CH_3-O interaction. Several examples and further details of manipulation experiments are given in the Supporting Information. The issue of the stabilizing interactions within the *squares* will be tackled later, after discussing the behavior of the system at higher temperatures.

Subsequent annealing of the surface up to 273 K leads to a further decrease in the molecular coverage and to the formation of a variety of complexes, which are summarized in Figure 4. In the same figure, high-resolution details of the four most common complexes are shown, whereas other minor variants to these configurations can be found on the surface (less than

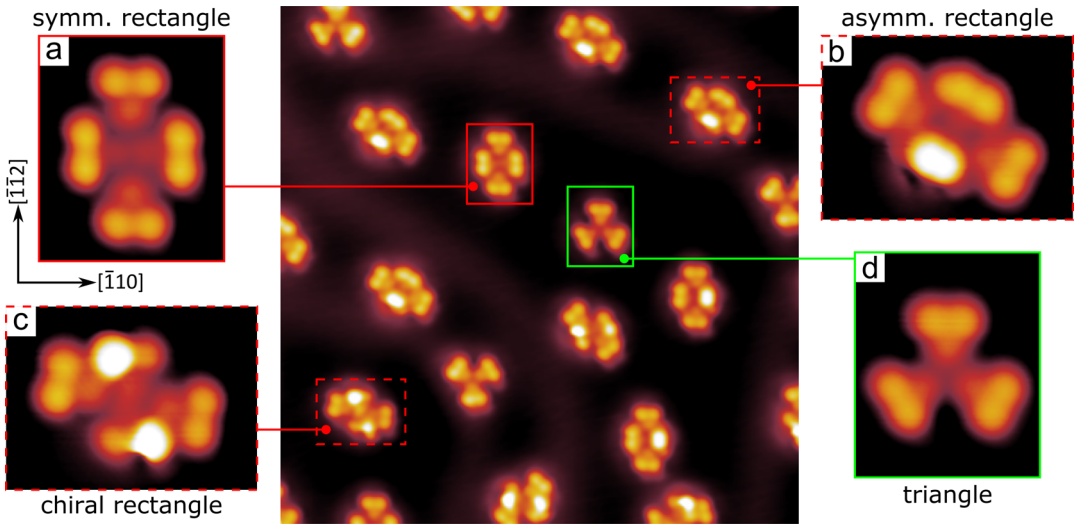

Figure 4. STM image (center, 12.94 × 12.94 nm^2) showing the various complexes that form on the surface after annealing to 273 K. (a–d) Insets show high resolution details of complexes: (a) the *rectangle* complex (1.63 × 1.99 nm^2), (b) the *asymmetric rectangle* complex (2.21 × 1.62 nm^2), (c) the *chiral rectangle* complex (2.21 × 1.62 nm^2) and (d) the *triangle* complex (1.63 × 1.99 nm^2). All images: 30 mV < V_s < 50 mV, 100 pA < I_t < 200 pA.

10% of the total number of complexes). While the arrangement of the DMSO molecules within the complexes in Figure 4a,d can be readily identified, since the shape of the single DMSO molecules is evident, the complexes in Figure 4b,c are less trivial to understand. More precisely, in the STM image in Figure 4b, three DMSO molecules can be readily identified, whereas the nature of the brighter protrusion is not straightforward. Similarly, in Figure 4c, two DMSO molecules can be recognized, whereas the assignment of the two brighter features needs further investigation. For sake of simplicity, from now on we shall refer to the complexes in Figure 4a–d as the *symmetric rectangle*, *asymmetric rectangle*, *chiral rectangle*, and *triangle*, respectively.

To better understand the nature of the observed bright protrusions, we have performed experiments involving the manipulation of the complexes as described for the *square*. In particular, Figure 5 shows the result of two subsequent voltage pulses applied at the location indicated by the green markers, in a sequence of STM images acquired from the same area. As can be observed, under voltage pulses, the *symmetric rectangle* can be converted back and forth into the *chiral rectangle*, unambiguously confirming that the constitutive units of both *rectangles* are the same, *i.e.*, four DMSO molecules.

As shown in the Supporting Information, together with various other examples of manipulation experiments, also the *asymmetric rectangle* could be converted to a *symmetric rectangle* and to a *chiral rectangle*, thereby indicating that the protrusion on the side of the former complex is likely a single DMSO in a different adsorption configuration.

Surprisingly enough, it appears that a common feature of all the described complexes is that the oxygen atoms appear to be preferentially located close

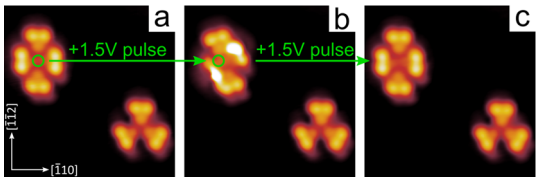

Figure 5. Sequence of STM images of the same area, showing the effect of +1.5 V voltage pulses applied with the STM tip at the location indicated by the green marker. A *symmetric rectangle* (a) is converted to a *chiral rectangle* (b) and eventually back to a *symmetric rectangle*. The *triangle* at the bottom right corner remains immobile in all three images, and acts as a reference. All images: V_s = 100 mV, I_t = 100 pA, 4.20 × 4.20 nm^2.

to each other, a configuration that should be extremely unfavorable due to the negative charge on the oxygens. To understand this behavior, we have carried out Density Functional Theory (DFT) calculations of the structural, electronic, and energetic properties of the observed DMSO complexes as well as simulations of the STM images. For sake of simplicity and computational cost, we started from the simplest complex, *i.e.*, the *triangle*. From the experimental STM images, it can be easily inferred that the complex is formed by three DMSO molecules with a measured distance of approximately twice the Au lattice constant between the S atoms. DFT calculations indicate that the most favorable adsorption configuration for a single adsorbed DMSO is the on-top site, with the S atom bound to the metal surface. As expected from the above chemical considerations, a *triangle* with all three DSMO adsorbed on top is predicted by DFT to be less stable (losing 0.13 eV/molecule) with respect to a single adsorbed DMSO taken as the reference configuration (1.78 eV/molecule). For the details of how the relevant energies are calculated, we refer the reader to the

discussion of Table 1 below. In this *triangle*, upon relaxation each DMSO rotates around the S atom by slightly more than 30° (the DFT-optimized structure is shown in the Supporting Information), in order to maximize the O–H interaction, in analogy to the behavior reported for the pure crystalline form.[58] To explain the stability of the structure, we have therefore hypothesized the presence of an Au adatom trapped within the complex, where it could act as an acceptor for the electrons of the oxygen atoms. As a consequence of this ansatz, the *triangle* becomes stable, gaining 0.25 eV/molecule with respect to single DMSO adsorption. In agreement with the experimental STM data, the simulated images clearly show no protrusion related to the adatom at the center of the complex, as can be seen in Figure 6d. It should be noted that in the experimental STM images the *triangles* can be found pointing in both the [11$\bar{2}$] and the [$\bar{1}\bar{1}$2] directions (see Figure 4). These two possible adsorption configurations of the *triangle* are consistent with the preferred adsorption site of DMSO (on-top), and with the two possible hollow Au sites for the adatom (*hcp* and *fcc*). Manipulation experiments described in the Supporting Information further support this picture: the minimum lateral displacement of the center of a *triangle*, upon switching its orientation with a voltage pulse, well agrees with the distance between two neighboring *hcp* and *fcc* sites for the adatom.

TABLE 1. Calculated Average Adsorption (E_{ads}) and Cohesion Energies (E_{coh}) per DMSO Molecule of the Various Molecular Complexes[a]

species	E_{ads}	E_{coh}
single DMSO	1.78	-
square	1.82	0.05
triangle	2.02	0.25
symm. rectangle	2.17	0.40
chiral rectangle	2.09	0.32
asymm. rectangle	2.11	0.35

[a] Energies in eV.

On the basis of the same chemical considerations used for the *triangle*, the stability of the *symmetric rectangle* can only be explained by introducing two Au adatoms, as shown in Figure 6a, gaining 0.40 eV/molecule with respect to a single adsorbed DMSO. Also in this case, the adatoms are not visible in the experimental STM images, and the absence of protrusions related to their presence is confirmed by the calculated image. The two adatoms are located in *fcc* and *hcp* hollow sites, and consistently with the C_3 symmetry of the substrate, they are observed with the long side oriented in all the three equivalent ⟨$\bar{1}\bar{1}$2⟩ directions.

With concern to the *asymmetric rectangle* and the *chiral rectangle*, various models have been tested, and the ones that show the best agreement with the experiment in terms of energetics and appearance of the STM images are shown in Figure 6b,c. The energetic gain, referred to a single adsorbed DMSO, is 0.35 and 0.32 eV/molecule, respectively.

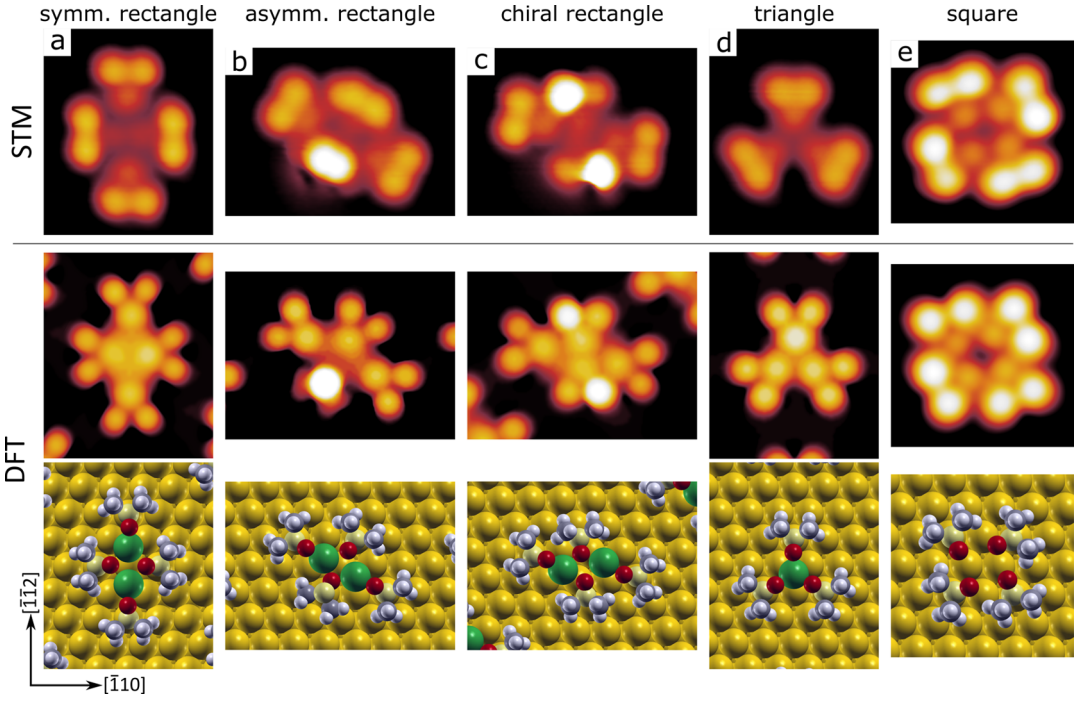

Figure 6. (a–e) STM images of the various DMSO complexes from Figures 4a–d and 3c, showing the experimental (top row) and the DFT calculated images (middle row). The bottom row shows ball models of the geometries obtained by DFT calculations, where the gold adatoms are painted in green to ease their identification. The lateral scales of the images within each column are the same, and are the same of Figure 4a–d and Figure 3c.

In the *asymmetric rectangle* (Figure 6b), the brighter protrusion is originated by a DMSO molecule in an "inverted" adsorption geometry, *i.e.*, with the S atom pointing out of the surface plane and the O atom interacting with the Au adatoms. As in the case of the *symmetric rectangle*, the two adatoms are located in *fcc* and *hcp* hollow sites, and the complexes can be found on the surface with the same orientations.

The *chiral rectangle* (Figure 6c) is again characterized by the presence of two adatoms in *fcc* and *hcp* hollow sites. However, in this case, the two sites are almost aligned along the [$\bar{1}$10] direction, with the adatoms located slightly off-site, giving rise to a characteristic angle of ±14° of the long side of the complex with respect to the equivalent ⟨$\bar{1}$10⟩ directions.

The simulated STM images in Figure 6a–d are in good agreement with the corresponding experimental images, since the morphology of the main features can be immediately identified, in particular concerning the lack of features related to the presence of the adatoms. However, it is also clear that the methyl groups in the simulated images always appear lower than the experimental ones. This artifact can be traced back to the pseudopotential used in our calculations, which underestimates the S–Au distance, inducing the methyl groups to relax to a slightly lower position, thus yielding a decrease in their contrast which is not observed in the experimental images (see Supporting Information for further details).

The case of the *square* complex deserves a separate discussion. Similarly to the other complexes, the oxygen atoms are quite close to each other, possibly giving rise to a repulsive interaction that could in principle destabilize the complex. However, in this case the molecular arrangement also favors the interaction between the oxygen and the methyl groups of each couple of adjacent molecules. The calculated CH–O angle in the closest H–O couple (2.5 Å) is approximately 140°, and this geometry does in fact favor the formation of a hydrogen bond.[63–65] Additionally, as mentioned above, the *square* exhibits a remarkable stability upon manipulation with the STM tip. Therefore, the question arises whether or not an adatom is trapped inside the complex, and the contrast of the STM images cannot address this point since we have verified that the trapped adatoms, even when present, are not visible both in the experimental and simulated STM images. To clarify this point, on one side we analyzed the distribution of the characteristic orientations of the complexes with respect to the Au(111) crystallographic directions in the experimental STM images, and on the other, we carefully evaluated the energetics of the different complexes as obtained by DFT.

As a starting point, we have measured the orientation of more than 1500 *square* complexes on the experimental STM images, using as a reference the directions shown as blue lines in the top inset of Figure 7.

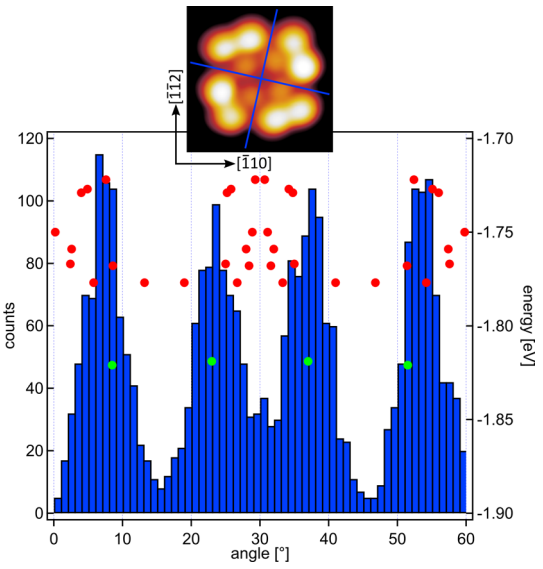

Figure 7. Experimental angular distribution of the *square* complexes (blue histogram, left axis) and the adsorption energy per molecule (markers, right axis) of the possible candidate models for the *square* complex with (red) and without (green) the central adatom. The thumbnail above the graph shows the directions taken as a reference to determine the orientation of the *square* complexes.

By taking into account both the symmetry of the substrate and the symmetry of the *square* complexes themselves, the resulting angular distribution of the complexes falls within 0° and 60° (see Supporting Information for details on the measurement of the angles), and is represented by the blue histogram in Figure 7 (left axis). It is clear that *squares* are aligned around four distinct angles, namely, 7°, 23°, 36°, and 53° with an error of about ±4°. In the same graph, the green and red markers show the calculated energies of various structures composed by four DMSO molecules (right axis), hypothesized as reasonable candidates for the *square* complex, as a function of their characteristic angle with respect to the surface. In particular, the red (green) markers correspond to the models including (excluding) the Au adatom. It is to be noted that relaxation of the models corresponding to the red markers after removal of the adatom consistently yielded one of the structures corresponding to the green marker.

Both analyses indicate that, at variance with the other observed complexes, the *squares* do not include a central gold adatom: First, from the energetic point of view, it is clear that the complexes with no adatom are always more stable (green markers) by more than 50 meV. Second, a clearly different angular distribution should be found if the *squares* included the adatoms (red markers). Details of the various models that have been simulated by DFT are shown in the Supporting Information.

The adsorption geometry of DMSO within the structures obtained from DFT calculations can also be

compared to the one inferred from the NEXAFS spectra. As pointed out earlier, the latter indicate an angle of 25° ± 10° between the S═O direction and the surface plane, a value thus fully compatible with all the calculated structures, where it lies between 25° and 32°. This result can be rationalized in the context of simple chemical considerations. The sulfur atom of DMSO has a tetrahedral coordination geometry, exposing an electron lone pair at the "tip" of the umbrella structure that characterizes the molecule. The angle between this pair and the S═O bond is roughly 110° for the free molecule. Considering that the binding to the metal substrate typically occurs through the lone pair (as in the case of ammonia,[66] for instance), the expected value of the angle between the S═O bond and the surface plane for the adsorbed molecule is about 20°, in agreement with our results.

It is to be noted that we have no direct information to pinpoint the process by which the DMSO complexes form, in particular concerning the actual origin of the adatom(s) in the complexes. However, in the temperature range where we observe adatoms trapped within complexes (*i.e.*, above 233 K), it is well-known that native gold adatoms can detach from step edges, diffuse along them and across the surface itself, as well as be extracted from the herringbone reconstruction and elbow sites.[37,67,68] Moreover, it is also well established that molecular adsorption, especially involving very electronegative species, can significantly promote such processes.[37,69] In contrast to thiols and other molecules that interact strongly with gold, in our case no lifting of the herringbone reconstruction was ever observed, likely because the interaction of DMSO with gold is comparatively weaker (no covalent bonding occurs between the molecule and the metal).

Table 1 shows the calculated average adsorption E_{ads} and cohesion E_{coh} energies per DMSO molecule of the various molecular complexes.

The adsorption energies have been calculated as

$$E_{ads}(n) = -\frac{1}{n}[E(n\text{DMSO}/sub) - n \times E(\text{DMSO}) - E(sub)]$$

where *sub* indicates the substrate, *i.e.*, the clean Au(111) surface, for the single DMSO and the *square,* or the surface with one or two Au adatoms, for the *triangle* and the *rectangles*; *n*DMSO indicates a DMSO complex with *n* molecules; *E*(*n*DMSO/*sub*), *E*(DMSO) and *E*(*sub*) indicate the energies of the total system (adsorbed complex and substrate), of a gas-phase, isolated DMSO molecule, and of the substrate, respectively. The cohesion energy per molecule, defined as

$$E_{coh}(n) = E_{ads}(n) - E_{ads}(1)$$

indicates the energy gain per DMSO molecule in the most stable adsorption configurations of a complex with respect to the adsorption of the individual molecule(s) on the bare Au(111) surface.

The energetics of the various complexes can help to rationalize the experimental observations. The least stable species is the single DMSO molecule (1.78 eV/molecule), that was in fact observed in rare cases. The *square* complex (1.82 eV/molecule) is more stable than the single adsorbed molecule, and is by far the dominant structure, together with the monolayer phase, at temperatures below 233 K (see Figure 3a). This is apparently in contrast with the fact that all the other complexes are significantly more stable than the *square* itself, and should therefore dominate the surface. However, as shown above, strong energetic and structural evidence indicate that this particular complex is the only one not entrapping one or more Au adatoms. It is reasonable to assume that at temperatures below 233 K a decreased availability of gold adatoms prevents the formation of *triangles* and *rectangles*, and therefore favors the formation of the *squares*. This consideration further strengthens the conclusion that no adatoms are trapped inside the *squares*.

The cohesion energies reported in Table 1 indicate that the presence of the adatoms in *triangles* and *rectangles* plays a relevant role in the stability of the complexes: molecule−molecule and molecule−adatom interactions (E_{coh}) account for 15−18% of their adsorption energies E_{ads}. This stabilization effect of the adatoms is also reflected in the fact that desorption of DMSO becomes more costly at increasing temperatures, as shown in the Supporting Information. Conversely, in the *squares*, E_{coh}/E_{ads} is only 3%, consistently with the weaker molecule−molecule hydrogen bonding.

DFT calculations also reveal that a peculiar redistribution of the electron density occurs around the Au adatom, as shown for the *triangle* by the charge density transfer plots in Figure 8. The latter have been calculated as $\rho_{tot}(\mathbf{r}) - \rho_{sub}(\mathbf{r}) - \sum\rho_{mol}(\mathbf{r})$, where $\rho_{tot}(\mathbf{r})$ is the charge density of the total system, $\rho_{sub}(\mathbf{r})$ the density of the gold substrate including an isolated adatom, and $\sum\rho_{mol}(\mathbf{r})$ the density of three noninteracting DMSO molecules in gas phase.

Namely, the density depletion (blue lobe) occurring at the gold adatom suggests that this atom displays a significant degree of cationic behavior. This is confirmed by the calculation of the atomic Löwdin charges:[70] even in the absence of DMSO coadsorption, a single Au adatom in the hollow position is always slightly positively charged ($\approx -0.21e^-$) with respect to an atom of the surface layer, by donating electronic charge to the nearest neighbor surface Au atoms. In the presence of a DMSO complex, the adatom recovers only part of its electronic charge ($\approx +0.08e^-$ relative to the single adatom) and rearranges the occupation of its s, p, and d orbitals. Moreover, at the same time,

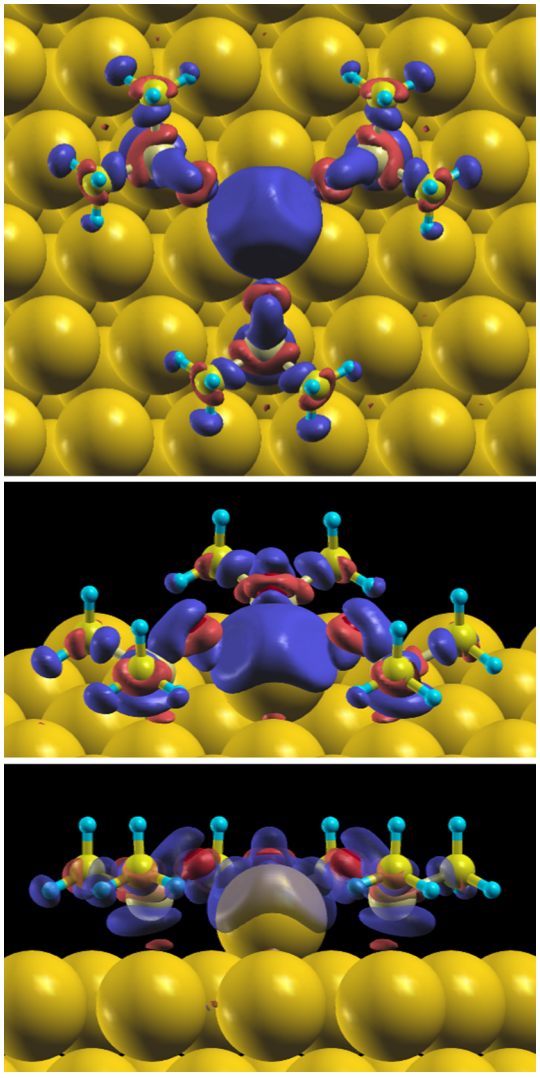

Figure 8. Top (top panel) and side (bottom panel) views of the changes in charge density around a gold adatom coordinated by three DMSO molecules (*triangle* complex) on the Au(111) surface with a pre-existing adatom on it. A perspective view (middle panel) is also shown. The accumulation of negative charge is depicted in red, the depletion in blue. The blue lobe surrounding the adatom highlights its cationic behavior.

an increase in the electronic charge occurs on its second nearest neighbor surface Au atoms, which are directly interacting with the sulfur of DMSO. The oxygen atoms surrounding the adatom are polarized in a characteristic double peak-trough pattern: this charge rearrangement pattern favors the coordination of the oxygen terminations of DMSO with the gold adatom, which effectively acts as ionic linker between the otherwise mutually repelling molecular terminations. The observed charge depletion and the proximity of deep p-orbitals associated with the oxygen atom ligands imply the lack of electron states available for tunneling in the STM observations at the Au site. This is consistent with the STM images where the adatom is indeed not visible. It is to be noted that linker adatoms which cannot be resolved in STM images were also reported in other works, and this effect was accompanied by a reduction of the occupation of the adatom states upon surface complexation.[32,41] It is important to remark that we have carried out extensive imaging on the complexes at various sample bias voltages, ranging from −3 up to +1 V. Within this interval, no significant contrast variations could be observed on the complexes, except for degradation of the resolution and broadening of the molecule-related protrusions. This observation gives experimental confirmation that no adatom-related electronic states are available for tunneling in the examined energy range. Measuring at bias voltages outside this range yielded very unstable imaging and easily induced changes in the complexes, even at very low tunneling current set points (≈1 pA), pointing out to possible, strong interactions between the tip−sample electric field and the molecular dipole. Eventually, it is to be noted that also the simulated images show no relevant contrast variation within the above-mentioned bias range, and the adatom-projected density of states is negligible in the corresponding energy interval.

Our finding of a significant charge redistribution around the presumably entrapped adatoms is analogous to what was observed by Pawin *et al.* for 9,10-anthracenedicarbonitrile on Cu(111), where a similar effect occurs.[71] Such charging effect could explain the reported increase in the reactivity of Au(111) surfaces covered by PDI metal−organic frameworks with respect to CO_2 and CO adsorption, compared to the bare Au(111) surface.[72,73] Notably, evidence has been found that charging is at the origin of the reactivity of small gold nanoclusters on metal oxide surfaces, for instance in reactions involving CO.[74−77]

Finally, we observe that the ionic character of the DMSO−adatom interaction is consistent with the average Au(adatom)−O distance, which is approximately 2.6 Å, and 30% larger than the same distance in related oxo-gold compounds (∼2.0 Å), where the Au−O bond is mainly covalent.[78]

A final comment is also due regarding the interpretation of the XPS spectra by the Su and Faller method mentioned above, according to which, from a negligible shift in ΔE_b (as we observe) a bidentate binding mode (S-metal and O-metal) would be expected at all the temperatures we have characterized. In contrast to this conclusion, our STM and DFT results indicate that at temperatures below 233 K there is no oxygen−metal bonding, but only O−CH_3 hydrogen bonds are formed. This observation points out to a limited applicability of the Su and Faller method, primarily because it does not consider the possibility of types of S- or O- interactions other than with the metal itself. In fact, in our case, it is evident that a similar shift in ΔE_b can be induced by O−metal or O−CH_3 interactions.

CONCLUSIONS

In the present work, we have shown that there is a mutual stabilization between a common, polar molecule, DMSO, and native, positively charged adatoms on the Au(111) surface. The existence of these adatoms, for which no directly related features are visible in the experimental data, is strongly supported by the agreement between the measured and simulated STM images, as well as by the observed stability of the complexes, that would remain otherwise unexplained. These adatoms act as ionic linkers between the molecules, a behavior reported up to now only for alkali metal linkers. The broader interest of any such mechanism stems from the evidence that, even at low coverage, fabricating discrete structures with high size selectivity can be achieved by exploiting more than just attractive short-range intermolecular interactions (*i.e.*, van der Waals, or H-bonding). In particular, it is gradually becoming clear that monodisperse cluster populations can be obtained if interactions of electrostatic nature are also present, as, for instance, repulsive interactions between parallel dipoles which act on a longer range.[79]

The observed mutual stabilization of DMSO and Au is likely related to the strong dipole moment of the molecule and the strong electronegativity of its constituents: further investigations are envisioned on the specific role of the sulfinyl group which could be exploited as a functional group to drive the assembly of more complex tectons through the described electrostatic linkage scheme, based on nondestructive extraction/stabilization of native metal atoms from the substrate.

The nanoscale properties of the Au−DMSO interface are also of great relevance in electrochemistry and, more generally, wet chemistry. For instance, a relatively strong DMSO−Au binding, as originated from our observed bidentate configuration, was hypothesized as a possible origin of the unusual behavior of liquid DMSO at noble metal electrodes.[55,56,80] Very recently, the ability of DMSO to act as a "functional solvent" in the synthesis of metal nanoparticles, advantageously providing in a single solvent the ability to both solvate and stabilize the gold aggregates, was tentatively explained by Duggan *et al.* with an enhanced S- and O-coordination to gold, on the basis of FT-IR spectra.[81] Clearly, a generalization of our results to the mentioned cases, where liquid−solid interfaces are involved, is far from straightforward, but further investigations at the liquid DMSO−Au interface could benefit from our findings.

METHODS

The Au(111) surface was cleaned by repeated Ne^+ or Ar^+ sputtering at 500 eV at room temperature for 20 min followed by annealing at 873 K for 20 min. Dimethyl sulfoxide (Sigma-Aldrich, anhydrous, ≥ 99%), was dosed on the Au sample by backfilling the UHV chamber through a leak valve connected to a glass vial, where DMSO was transferred under nitrogen atmosphere to prevent water contamination. Before dosing in the UHV chamber, DMSO was thoroughly cleaned by means of several freeze−pump−thaw cycles. The DMSO adsorption phases were prepared by exposing the sample held at 153 K to a background pressure of DMSO of about 4×10^{-6} Pa for about 15 s. This preparation consistently yielded a multilayer phase. Monolayer and submonolayer phases were then prepared by simply heating the multilayer phase or by dosing at saturation at a specific sample temperature. We verified that no difference could be observed in the final surface by using the two alternative preparation methods.

Scanning Tunneling Microscopy. Low temperature STM measurements were carried out with an Omicron LT-STM system, at a temperature of approximately 4 K. The microscope is hosted in a UHV chamber, operating at a base pressure of about 1×10^{-8} Pa. Images were acquired in the constant current mode, with the bias voltage applied to the sample and the tip at ground. Electrochemically etched tungsten tips were used. STM images were processed by subtracting a background plane to correct for the sample tilting.[82] The applied enhancements consist of B-spline resampling, to increase the sample count, and mild Gaussian filtering, to remove high frequency noise components.

Photoelectron Spectroscopy. XPS and NEXAFS measurements were carried out at the ALOISA beamline of the ELETTRA synchrotron light source (Trieste, Italy).[83] O 1s and S 2p XPS spectra were acquired at $h\nu = 650$ eV with an overall resolution of 0.35 eV. The binding energy scale has been calibrated with respect to the bulk spectral component of the Au $4f_{7/2}$ peak at 84.0 eV.[84] NEXAFS spectra were acquired in electron partial yield with a photon energy resolution of 0.15 eV.

Theoretical Calculations. DFT calculations were performed with the plane-wave pseudopotential package QUANTUM ESPRESSO,[85] using ultrasoft pseudopotentials[86] with a wave function (charge) energy cutoff of 408 eV and a GGA-PBE[87] exchange-correlation functional. Since van der Waals interactions play a non-negligible role in self-assembled organic structures, we adopted the semiempirical dispersion-corrected DFT (DFT-D) method proposed by Grimme,[88] recently implemented in the QE package[89] and successfully used by Casarin *et al.* to determine the adsorption energetics of iron phthalocyanine on Ag(110).[90] Brillouin-zone sampling included two *k* points in *x* and *y* directions, and only one in *z* direction, perpendicular to the surface. The Au(111) surface was modeled with three layers for the simulations of the DMSO complexes and four layers for the monolayer simulation (see Supporting Information), allowing a vacuum (adlayer−surface) distance of ≈1.2 nm. The bottom layer of the surface was kept fixed at the bulk Au calculated values to mimic the behavior of the metal substrate. In the presence of the surface, only forces acting on the top Au layer and the molecular adlayer atoms were relaxed. Forces were relaxed up to 0.26 eV/Å.

STM images were simulated within the Tersoff-Hamann approximation according to which the tunneling current is proportional to the energy-Integrated electronic Local Density Of States (ILDOS).[91] To mimic the constant-current experimental STM images, we map an ILDOS iso-surface lying within a certain height range over the surface. All the images in this work were simulated at a bias of 100 mV, at an ILDOS value for the iso-surface of 4×10^{-3} nm^{-3}, lying at an average distance of approximately 0.5 nm from the first atomic layer. Ball models are rendered with the XCrySDen, Avogadro and POV-Ray software packages.[92−95]

Conflict of Interest: The authors declare no competing financial interest.

Supporting Information Available: Additional STM manipulation experiments, temperature dependence of the molecular complexes, further details on the X-ray spectroscopic data and the theoretical calculations. The Supporting Information is available free of charge on the ACS Publications website at DOI: 10.1021/acsnano.5b02284.

Acknowledgment. We gratefully acknowledge Federico Berti and Ambra Dreos for fruitful discussions on the chemistry of DMSO. C.D., A.C., Z.F., and C.C.-C. acknowledge financial support from MIUR through Futuro in Ricerca – FIRB 2010 Project No. RBFR10FQBL. A.D.V. acknowledges support from the EPSRC Grant EP/G044864/1 in the early stages of this work. S.V. acknowledges computing resources made available at the CINECA HPC facility through the UTS-CINECA Convention. M.P. acknowledges financial support from the Italian Ministry of Foreign Affairs and International Cooperation, Directorate General for the Country Promotion (Project PGR00190).

REFERENCES AND NOTES

1. Barth, J. V. Molecular Architectonic on Metal Surfaces. *Annu. Rev. Phys. Chem.* **2007**, *58*, 375–407.
2. De Feyter, S.; De Schryver, F. C. Two-Dimensional Supramolecular Self-Assembly Probed by Scanning Tunneling Microscopy. *Chem. Soc. Rev.* **2003**, *32*, 139–150.
3. Bartels, L. Tailoring Molecular Layers at Metal Surfaces. *Nat. Chem.* **2010**, *2*, 87–95.
4. Haq, S.; Hanke, F.; Sharp, J.; Persson, M.; Amabilino, D. B.; Raval, R. Versatile Bottom-Up Construction of Diverse Macromolecules on a Surface Observed by Scanning Tunneling Microscopy. *ACS Nano* **2014**, *8*, 8856–8870.
5. Simard, M.; Su, D.; Wuest, J. D. Use of Hydrogen Bonds to Control Molecular Aggregation. Self-Assembly of Three-Dimensional Networks with Large Chambers. *J. Am. Chem. Soc.* **1991**, *113*, 4696–4698.
6. Desiraju, G. R. Supramolecular Synthons in Crystal Engineering—A New Organic Synthesis. *Angew. Chem., Int. Ed. Engl.* **1995**, *34*, 2311–2327.
7. Clair, S.; Pons, S.; Seitsonen, A. P.; Brune, H.; Kern, K.; Barth, J. V. STM Study of Terephthalic Acid Self-Assembly on Au(111): Hydrogen-Bonded Sheets on an Inhomogeneous Substrate †. *J. Phys. Chem. B* **2004**, *108*, 14585–14590.
8. Yokoyama, T.; Kamikado, T.; Yokoyama, S.; Mashiko, S. Conformation Selective Assembly of Carboxyphenyl Substituted Porphyrins on Au (111). *J. Chem. Phys.* **2004**, *121*, 11993–11997.
9. Otero, R.; Schöck, M.; Molina, L. M.; Lægsgaard, E.; Stensgaard, I.; Hammer, B.; Besenbacher, F. Guanine Quartet Networks Stabilized by Cooperative Hydrogen Bonds. *Angew. Chem.* **2005**, *117*, 2310–2315.
10. Feng, Z.; Cudia, C. C.; Floreano, L.; Morgante, A.; Comelli, G.; Dri, C.; Cossaro, A. A Competitive Amino-Carboxylic Hydrogen Bond on a Gold Surface. *Chem. Commun.* **2015**, *51*, 5739–5742.
11. Dmitriev, A.; Spillmann, H.; Lin, N.; Barth, J. V.; Kern, K. Modular Assembly of Two-Dimensional Metal–Organic Coordination Networks at a Metal Surface. *Angew. Chem.* **2003**, *115*, 2774–2777.
12. Garah, M. E.; Ciesielski, A.; Marets, N.; Bulach, V.; Hosseini, M. W.; Samorì, P. Molecular Tectonics Based Nanopatterning of Interfaces with 2D Metal–Organic Frameworks (MOFs). *Chem. Commun.* **2014**, *50*, 12250–12253.
13. Stepanow, S.; Lin, N.; Barth, J. V. Modular Assembly of Low-Dimensional Coordination Architectures on Metal Surfaces. *J. Phys.: Condens. Matter* **2008**, *20*, 184002.
14. Faraggi, M. N.; Jiang, N.; Gonzalez-Lakunza, N.; Langner, A.; Stepanow, S.; Kern, K.; Arnau, A. Bonding and Charge Transfer in Metal–Organic Coordination Networks on Au(111) with Strong Acceptor Molecules. *J. Phys. Chem. C* **2012**, *116*, 24558–24565.
15. Yang, Z.; Corso, M.; Robles, R.; Lotze, C.; Fitzner, R.; Mena-Osteritz, E.; Bäuerle, P.; Franke, K. J.; Pascual, J. I. Orbital Redistribution in Molecular Nanostructures Mediated by Metal–Organic Bonds. *ACS Nano* **2014**, *8*, 10715–10722.
16. Everitt, D. L.; Miller, W. J. W.; Abbott, N. L.; Zhu, X. D. Evolution of a Preferred Orientation of Polycrystalline Grains in Obliquely Deposited Gold Films on an Amorphous Substrate. *Phys. Rev. B* **2000**, *62*, R4833–R4836.
17. Wang, Y.; Teitel, S.; Dellago, C. Melting of Icosahedral Gold Nanoclusters from Molecular Dynamics Simulations. *J. Chem. Phys.* **2005**, *122*, 214722.
18. Freakley, S. J.; He, Q.; Kiely, C. J.; Hutchings, G. J. Gold Catalysis: A Reflection on Where We Are Now. *Catal. Lett.* **2014**, *145*, 71–79.
19. Laguna, A. *Modern Supramolecular Gold Chemistry: Gold-Metal Interactions and Applications*; John Wiley & Sons: Weinheim, Germany, 2008.
20. Zhou, K.; Jia, J.; Li, C.; Xu, H.; Zhou, J.; Luo, G.; Wei, F. A Low Content Au-Based Catalyst for Hydrochlorination of C_2H_2 and Its Industrial Scale-Up for Future PVC Processes. *Green Chem.* **2014**, *17*, 356–364.
21. Dorsey, J. F.; Sun, L.; Joh, D. Y.; Witztum, A.; Kao, G. D.; Alonso-Basanta, M.; Avery, S.; Hahn, S. M.; Al Zaki, A.; Tsourkas, A. Gold Nanoparticles in Radiation Research: Potential Applications for Imaging and Radiosensitization. *Transl. Cancer Res.* **2013**, *2*, 280–291.
22. Chen, M. S.; Goodman, D. W. The Structure of Catalytically Active Gold on Titania. *Science* **2004**, *306*, 252–255.
23. Choudhary, T. V.; Goodman, D. W. Catalytically Active Gold: The Role of Cluster Morphology. *Appl. Catal. Gen.* **2005**, *291*, 32–36.
24. Wittstock, A.; Bäumer, M. Catalysis by Unsupported Skeletal Gold Catalysts. *Acc. Chem. Res.* **2013**, *47*, 731–739.
25. Harten, U.; Lahee, A. M.; Toennies, J. P.; Wöll, C. Observation of a Soliton Reconstruction of Au(111) by High-Resolution Helium-Atom Diffraction. *Phys. Rev. Lett.* **1985**, *54*, 2619–2622.
26. Barth, J. V.; Brune, H.; Ertl, G.; Behm, R. J. Scanning Tunneling Microscopy Observations on the Reconstructed Au(111) Surface: Atomic Structure, Long-Range Superstructure, Rotational Domains, and Surface Defects. *Phys. Rev. B* **1990**, *42*, 9307–9318.
27. Boscoboinik, J. A.; Calaza, F. C.; Habeeb, Z.; Bennett, D. W.; Stacchiola, D. J.; Purino, M. A.; Tysoe, W. T. One-Dimensional Supramolecular Surface Structures: 1,4-Diisocyanobenzene on Au(111) Surfaces. *Phys. Chem. Chem. Phys.* **2010**, *12*, 11624–11629.
28. Jewell, A. D.; Tierney, H. L.; Sykes, E. C. H. Gently Lifting Gold's Herringbone Reconstruction: Trimethylphosphine on Au(111). *Phys. Rev. B* **2010**, *82*, 205401.
29. Jewell, A. D.; Sykes, E. C. H.; Kyriakou, G. Molecular-Scale Surface Chemistry of a Common Metal Nanoparticle Capping Agent: Triphenylphosphine on Au(111). *ACS Nano* **2012**, *6*, 3545–3552.
30. Mielke, J.; Hanke, F.; Peters, M. V.; Hecht, S.; Persson, M.; Grill, L. Adatoms underneath Single Porphyrin Molecules on Au(111). *J. Am. Chem. Soc.* **2015**, *137*, 1844–1849.
31. Saywell, A.; Greń, W.; Franc, G.; Gourdon, A.; Bouju, X.; Grill, L. Manipulating the Conformation of Single Organometallic Chains on Au(111). *J. Phys. Chem. C* **2014**, *118*, 1719–1728.
32. Shi, Z.; Lin, N. Porphyrin-Based Two-Dimensional Coordination Kagome Lattice Self-Assembled on a Au(111) Surface. *J. Am. Chem. Soc.* **2009**, *131*, 5376–5377.
33. Zhang, H.; Franke, J.-H.; Zhong, D.; Li, Y.; Timmer, A.; Arado, O. D.; Mönig, H.; Wang, H.; Chi, L.; Wang, Z.; et al. Surface Supported Gold–Organic Hybrids: On-Surface Synthesis and Surface Directed Orientation. *Small* **2013**, 1361–1368.
34. Jewell, A. D.; Tierney, H. L.; Zenasni, O.; Lee, T. R.; Sykes, E. C. H. Asymmetric Thioethers as Building Blocks for Chiral Monolayers. *Top. Catal.* **2011**, *54*, 1357–1367.
35. Bellisario, D. O.; Jewell, A. D.; Tierney, H. L.; Baber, A. E.; Sykes, E. C. H. Adsorption, Assembly, and Dynamics of Dibutyl Sulfide on Au(111). *J. Phys. Chem. C* **2010**, *114*, 14583–14589.
36. Cossaro, A.; Mazzarello, R.; Rousseau, R.; Casalis, L.; Verdini, A.; Kohlmeyer, A.; Floreano, L.; Scandolo, S.; Morgante, A.; Klein, M. L.; et al. X-Ray Diffraction and Computation Yield the Structure of Alkanethiols on Gold(111). *Science* **2008**, *321*, 943–946.

37. Maksymovych, P.; Voznyy, O.; Dougherty, D. B.; Sorescu, D. C.; Yates, J. T. Gold Adatom as a Key Structural Component in Self-Assembled Monolayers of Organosulfur Molecules on Au(111). *Prog. Surf. Sci.* **2010**, *85*, 206–240.
38. Häkkinen, H. The Gold−Sulfur Interface at the Nanoscale. *Nat. Chem.* **2012**, *4*, 443–455.
39. Olmos-Asar, J. A.; Ludueña, M.; Mariscal, M. M. Monolayer Protected Gold Nanoparticles: The Effect of the Headgroup−Au Interaction. *Phys. Chem. Chem. Phys.* **2014**, *16*, 15979–15987.
40. Olmos-Asar, J. A.; Rapallo, A.; Mariscal, M. M. Development of a Semiempirical Potential for Simulations of Thiol−Gold Interfaces. Application to Thiol-Protected Gold Nanoparticles. *Phys. Chem. Chem. Phys.* **2011**, *13*, 6500–6506.
41. Classen, T.; Fratesi, G.; Costantini, G.; Fabris, S.; Stadler, F. L.; Kim, C.; de Gironcoli, S.; Baroni, S.; Kern, K. Templated Growth of Metal−Organic Coordination Chains at Surfaces. *Angew. Chem., Int. Ed.* **2005**, *44*, 6142–6145.
42. Tseng, T.-C.; Abdurakhmanova, N.; Stepanow, S.; Kern, K. Hierarchical Assembly and Reticulation of Two-Dimensional Mn- and Ni−TCNQx (x = 1, 2, 4) Coordination Structures on a Metal Surface. *J. Phys. Chem. C* **2011**, *115*, 10211–10217.
43. Abdurakhmanova, N.; Floris, A.; Tseng, T.-C.; Comisso, A.; Stepanow, S.; De Vita, A.; Kern, K. Stereoselectivity and Electrostatics in Charge-Transfer Mn- and Cs-TCNQ4 Networks on Ag(100). *Nat. Commun.* **2012**, *3*, 940.
44. Floris, A.; Comisso, A.; De Vita, A. Fine-Tuning the Electrostatic Properties of an Alkali-Linked Organic Adlayer on a Metal Substrate. *ACS Nano* **2013**, *7*, 8059–8065.
45. Smallwood, I. M. *Handbook of Organic Solvent Properties*; Arnold; Halsted Press: London; New York, 1996.
46. Kvakovszky, G.; McKim, A.; Moore, J. C. A Review of Microelectronic Manufacturing Applications Using DMSO-Based Chemistries. *ECS Trans.* **2007**, *11*, 227–234.
47. Zhu, P.; Chen, Y.; Wang, L.; Qian, G.; Zhang, W. J.; Zhou, M.; Zhou, J. Dissolution of Brominated Epoxy Resins by Dimethyl Sulfoxide To Separate Waste Printed Circuit Boards. *Environ. Sci. Technol.* **2013**, *47*, 2654–2660.
48. Ashwood-Smith, M. J. Current Concepts Concerning Radioprotective and Cryoprotective Properties of Dimethyl Sulfoxide in Cellular Systems. *Ann. N.Y. Acad. Sci.* **1975**, *243*, 246–256.
49. Thong, H.-Y.; Zhai, H.; Maibach, H. I. Percutaneous Penetration Enhancers: An Overview. *Skin Pharmacol. Physiol.* **2007**, *20*, 272–282.
50. Schröter, C.; Roelfs, B.; Solomun, T. The Interaction of Dimethylsulfoxide with a Gold Surface. *Surf. Sci.* **1997**, *380*, L441–L445.
51. Ikemiya, N.; Gewirth, A. A. Structure Sensitive Adsorption of DMSO on Au Surfaces. *J. Phys. Chem. B* **2000**, *104*, 873–877.
52. Sexton, B. A.; Avery, N. R.; Turney, T. W. A Spectroscopic Study of the Coordination of Dimethyl Sulfoxide to a Platinum (111) Surface. *Surf. Sci.* **1983**, *124*, 162–174.
53. Garwood, G. A., Jr; Hubbard, A. T. Superlattices Formed by Interaction of Polar Solvents with Pt (111) Surfaces Studied by LEED, Auger Spectroscopy and Thermal Desorption Mass Spectrometry. *Surf. Sci.* **1982**, *118*, 223–247.
54. Si, S. K.; Gewirth, A. A. Complex Formation between Halogens and Sulfoxides on Metal Surfaces. *Phys. Chem. Chem. Phys.* **2001**, *3*, 3325–3329.
55. Roelfs, B.; Schröter, C.; Solomun, T. A Comparison of Metal/Vacuum and Metal/Electrolyte Interfaces: The Au(100)/(Dimethylsulfoxide) and (Dimethylsulfoxide + Acetonitrile) Systems. *Berichte Bunsen-Ges. Phys. Chem.* **1997**, *101*, 1105–1112.
56. Si, S. K.; Gewirth, A. A. Solvent Organization above Metal Surfaces: Ordering of DMSO on Au. *J. Phys. Chem. B* **2000**, *104*, 10775–10782.
57. Su, C.-C.; Faller, J. W. Application of Electron Spectroscopy for Chemical Analysis to the Study of Ambidentate Binding in Sulfoxide Complexes. *Inorg. Chem.* **1974**, *13*, 1734–1736.
58. Thomas, R.; Shoemaker, C. B.; Eriks, K. The Molecular and Crystal Structure of Dimethyl Sulfoxide, $(H_3C)_2$ SO. *Acta Crystallogr.* **1966**, *21*, 12–20.
59. Leite, T. C. M.; de Barros, A. L. F.; Ferreira, G. B.; Guerra, A. C. O.; Turci, C. C. Photoabsorption Spectroscopy of Dimethyl Sulfoxide at the O1s, C1s, S2s, and S2p Regions: A Comparison with Acetone. *Int. J. Quantum Chem.* **2012**, *112*, 3421–3433.
60. Atak, K.; Engel, N.; Lange, K. M.; Golnak, R.; Gotz, M.; Soldatov, M.; Rubensson, J.-E.; Kosugi, N.; Aziz, E. F. The Chemical Bond in Carbonyl and Sulfinyl Groups Studied by Soft X-Ray Spectroscopy and *ab Initio* Calculations. *ChemPhysChem* **2012**, *13*, 3106–3111.
61. Sze, K. H.; Brion, C. E.; Tronc, M.; Bodeur, S.; Hitchcock, A. P. Inner and Valence Shell Electronic Excitation of Dimethyl Sulfoxide by Electron Energy Loss and Photoabsorption Spectroscopies. *Chem. Phys.* **1988**, *121*, 279–297.
62. Stöhr, J. *NEXAFS Spectroscopy*; Springer Series in Surface Sciences; Springer-Verlag: Berlin, 1992; Vol. 25.
63. Knak Jensen, S. J.; Tang, T.-H.; Csizmadia, I. G. Hydrogen-Bonding Ability of a Methyl Group. *J. Phys. Chem. A* **2003**, *107*, 8975–8979.
64. Cepellotti, A.; Peronio, A.; Marchini, S.; Abdurakhmanova, N.; Dri, C.; Africh, C.; Esch, F.; Comelli, G.; Peressi, M. NH_3−NO Coadsorption System on Pt(111). II. Intermolecular Interaction. *J. Phys. Chem. C* **2013**, *117*, 21196–21202.
65. Desiraju, G. R. The C−H···O Hydrogen Bond: Structural Implications and Supramolecular Design. *Acc. Chem. Res.* **1996**, *29*, 441–449.
66. Peronio, A.; Cepellotti, A.; Marchini, S.; Abdurakhmanova, N.; Dri, C.; Africh, C.; Esch, F.; Peressi, M.; Comelli, G. NH_3−NO Coadsorption System on Pt(111). I. Structure of the Mixed Layer. *J. Phys. Chem. C* **2013**, *117*, 21186–21195.
67. Stoltze, P. Simulation of Surface Defects. *J. Phys.: Condens. Matter* **1994**, *6*, 9495.
68. Zhang, J.-M.; Song, X.-L.; Zhang, X.-J.; Xu, K.-W.; Ji, V. Atomistic Simulation of Point Defects at Low-Index Surfaces of Noble Metals. *Surf. Sci.* **2006**, *600*, 1277–1282.
69. Baker, T. A.; Kaxiras, E.; Friend, C. M. Insights from Theory on the Relationship between Surface Reactivity and Gold Atom Release. *Top. Catal.* **2010**, *53*, 365–377.
70. Löwdin, P.-O. Quantum Theory of Many-Particle Systems. I. Physical Interpretations by Means of Density Matrices, Natural Spin-Orbitals, and Convergence Problems in the Method of Configurational Interaction. *Phys. Rev.* **1955**, *97*, 1474–1489.
71. Pawin, G.; Wong, K. L.; Kim, D.; Sun, D.; Bartels, L.; Hong, S.; Rahman, T. S.; Carp, R.; Marsella, M. A Surface Coordination Network Based on Substrate-Derived Metal Adatoms with Local Charge Excess. *Angew. Chem., Int. Ed.* **2008**, *47*, 8442–8445.
72. Boscoboinik, J.; Kestell, J.; Garvey, M.; Weinert, M.; Tysoe, W. T. Creation of Low-Coordination Gold Sites on Au(111) Surface by 1,4-Phenylene Diisocyanide Adsorption. *Top. Catal.* **2011**, *54*, 20–25.
73. Feng, M.; Sun, H.; Zhao, J.; Petek, H. Self-Catalyzed Carbon Dioxide Adsorption by Metal-Organic Chains on Gold Surfaces. *ACS Nano* **2014**, *8*, 8644–8652.
74. Rim, K. T.; Eom, D.; Liu, L.; Stolyarova, E.; Raitano, J. M.; Chan, S.-W.; Flytzani-Stephanopoulos, M.; Flynn, G. W. Charging and Chemical Reactivity of Gold Nanoparticles and Adatoms on the (111) Surface of Single-Crystal Magnetite: A Scanning Tunneling Microscopy/Spectroscopy Study. *J. Phys. Chem. C* **2009**, *113*, 10198–10205.
75. Chrétien, S.; Metiu, H. Density Functional Study of the Charge on Aun Clusters (n=1−7) Supported on a Partially Reduced Rutile TiO_2(110): Are All Clusters Negatively Charged? *J. Chem. Phys.* **2007**, *126*, 104701.
76. Wörz, A. S.; Heiz, U.; Cinquini, F.; Pacchioni, G. Charging of Au Atoms on TiO_2 Thin Films from CO Vibrational Spectroscopy and DFT Calculations. *J. Phys. Chem. B* **2005**, *109*, 18418–18426.
77. Baker, T. A.; Liu, X.; Friend, C. M. The Mystery of Gold's Chemical Activity: Local Bonding, Morphology and Reactivity of Atomic Oxygen. *Phys. Chem. Chem. Phys.* **2010**, *13*, 34–46.
78. Bauer, A.; Schier, A.; Schmidbaur, H. Methyldiphenylphosphine) (trimethylsiloxy) Gold(I). *Acta Crystallogr. C* **1995**, *51*, 2030–2032.

79. Kervyn, S.; Kalashnyk, N.; Riello, M.; Moreton, B.; Tasseroul, J.; Wouters, J.; Jones, T. S.; De Vita, A.; Costantini, G.; Bonifazi, D. "Magic" Surface Clustering of Borazines Driven by Repulsive Intermolecular Forces. *Angew. Chem., Int. Ed.* **2013**, *52*, 7410–7414.
80. Borkowska, Z.; Hamelin, A. The Influence of the Crystallographic Orientation on the Double Layer Parameters of the Au/Dimethylsulfoxide Interface. *J. Electroanal. Chem. Interfacial Electrochem.* **1988**, *241*, 373–377.
81. Duggan, J. N.; Roberts, C. B. Aggregation and Precipitation of Gold Nanoparticle Clusters in Carbon Dioxide-Gas-Expanded Liquid Dimethyl Sulfoxide. *J. Phys. Chem. C* **2014**, *118*, 14595–14605.
82. Nečas, D.; Klapetek, P. Gwyddion: An Open-Source Software for SPM Data Analysis. *Cent. Eur. J. Phys.* **2012**, *10*, 181–188.
83. Floreano, L.; Naletto, G.; Cvetko, D.; Gotter, R.; Malvezzi, M.; Marassi, L.; Morgante, A.; Santaniello, A.; Verdini, A.; Tommasini, F.; et al. Performance of the Grating-Crystal Monochromator of the ALOISA Beamline at the Elettra Synchrotron. *Rev. Sci. Instrum.* **1999**, *70*, 3855–3864.
84. Cossaro, A.; Floreano, L.; Verdini, A.; Casalis, L.; Morgante, A. Comment on "Local Methylthiolate Adsorption Geometry on Au(111) from Photoemission Core-Level Shifts". *Phys. Rev. Lett.* **2009**, *103*, 119601.
85. Giannozzi, P.; Baroni, S.; Bonini, N.; Calandra, M.; Car, R.; Cavazzoni, C.; Ceresoli, D.; Chiarotti, G. L.; Cococcioni, M.; Dabo, I.; et al. QUANTUM ESPRESSO: A Modular and Open-Source Software Project for Quantum Simulations of Materials. *J. Phys.: Condens. Matter* **2009**, *21*, 395502.
86. Vanderbilt, D. Soft Self-Consistent Pseudopotentials in a Generalized Eigenvalue Formalism. *Phys. Rev. B* **1990**, *41*, 7892–7895.
87. Perdew, J. P.; Burke, K.; Ernzerhof, M. Generalized Gradient Approximation Made Simple. *Phys. Rev. Lett.* **1996**, *77*, 3865.
88. Grimme, S. Semiempirical GGA-Type Density Functional Constructed with a Long-Range Dispersion Correction. *J. Comput. Chem.* **2006**, *27*, 1787–1799.
89. Barone, V.; Casarin, M.; Forrer, D.; Pavone, M.; Sambi, M.; Vittadini, A. Role and Effective Treatment of Dispersive Forces in Materials: Polyethylene and Graphite Crystals as Test Cases. *J. Comput. Chem.* **2009**, *30*, 934–939.
90. Casarin, M.; Marino, M. D.; Forrer, D.; Sambi, M.; Sedona, F.; Tondello, E.; Vittadini, A.; Barone, V.; Pavone, M. Coverage-Dependent Architectures of Iron Phthalocyanine on Ag(110): A Comprehensive STM/DFT Study. *J. Phys. Chem. C* **2010**, *114*, 2144–2153.
91. Tersoff, J.; Hamann, D. R. Theory of the Scanning Tunneling Microscope. *Phys. Rev. B* **1985**, *31*, 805–813.
92. Kokalj, A. Computer Graphics and Graphical User Interfaces as Tools in Simulations of Matter at the Atomic Scale. *Comput. Mater. Sci.* **2003**, *28*, 155–168.
93. Avogadro: an open-source molecular builder and visualization tool. Version 1.1.1. http://avogadro.openmolecules.net/.
94. Hanwell, M. D.; Curtis, D. E.; Lonie, D. C.; Vandermeersch, T.; Zurek, E.; Hutchison, G. R. Avogadro: An Advanced Semantic Chemical Editor, Visualization, and Analysis Platform. *J. Cheminf.* **2012**, *4*, 17.
95. Persistence of Vision Pty. Ltd (2004), Persistence of Vision Raytracer (Version 3.6), retrieved from http://www.povray.org/download/.